Pre-event water contributions to runoff events of different magnitude in pre-alpine headwaters

Benjamin M. C. Fischer, Manfred Stähli and Jan Seibert

ABSTRACT

Precipitation and catchment characteristics of mountainous headwaters can vary largely within short distances. It remains unclear how these two factors determine the contribution of event water and pre-event water to stormflow. We investigated this in five neighboring headwaters with high annual precipitation amounts (>2,000 mm y^{-1}) in a steep pre-alpine region in Switzerland. Rainfall and streamwater of 13 different rainstorms were sampled (P: 5 mm intervals, Q: 12 to 51 samples per events) to perform a two-component isotope hydrograph separation. Pre-event water contributions based on $\delta^{18}O$ or $\delta^{2}H$ computation were similar. The pre-event water contributions of headwaters depended largely on rainfall (amount and intensity) and varied more between events than between catchments, despite clear differences in land cover between the catchments. Furthermore, antecedent wetness was not found to control pre-event water contribution. With increasing rainfall amount, the proportion of rainfall in runoff increased and changed from pre-event to event water dominated. The variable rainfall amount and small active storage (organic soil horizon, 20–50 cm) resulted in a threshold in the upper soil horizon with subsequently more variable pre-event water contribution. Our results show the necessity of sampling in different headwaters and events to better understand controlling factors in runoff generation.

Key words | catchment comparison, headwater catchments, hydrograph separation, isotope hydrology, runoff generation

Benjamin M. C. Fischer (corresponding author)
Jan Seibert
Department of Geography,
University of Zurich,
Winterthurerstrasse 190,
CH-8057 Zurich,
Switzerland
E-mail: *benjamin.fischer@geo.uzh.ch*

Manfred Stähli
Swiss Federal Institute for Forest,
Snow and Landscape Research WSL,
Birmensdorf,
Switzerland

Jan Seibert
Department of Earth Sciences,
Uppsala University,
Uppsala,
Sweden

INTRODUCTION

Runoff generation processes vary in space and time. The spatial variation is controlled by catchment properties such as land-use/cover and geology, while the temporal variation is mainly controlled by hydrometeorological conditions such as precipitation and soil moisture. Understanding this spatiotemporal variability of runoff processes as a function of precipitation and catchment characteristics is important for predictions of streamflow quantity and quality.

As part of the water itself, the stable isotopes $\delta^{18}O$ and $\delta^{2}H$, are valuable conservative tracers in the two end-member mass balance approach (also called two-component isotope hydrograph separation (IHS)) to study how catchments transform rainfall into runoff. Using IHS allows the stormflow hydrograph to be separated, and to discern to what degree rainfall (event water) and water, that has been stored in the catchment before the event (pre-event water), contribute to stormflow (Sklash *et al.* 1976; Klaus & McDonnell 2013).

IHS has, however, frequently been performed only in single headwaters (e.g., McDonnell *et al.* 1990; Jordan 1994; Vitvar & Balderer 1997; Renshaw *et al.* 2003; Pellerin *et al.* 2008; Lyon *et al.* 2008; Penna *et al.* 2014). From several IHS studies in forested headwaters, the general perception developed that pre-event water dominates the peak discharge (Buttle 1994; Klaus & McDonnell 2013). However, the value of an IHS study in one catchment and one event is limited. Such studies are criticized for not providing further

doi: 10.2166/nh.2016.176

insights into hydrological processes (Burns 2002). With advances in laser spectroscopes, measuring the composition of both stable isotopes $\delta^{18}O$ and $\delta^{2}H$ has become relatively easy and the price per sample has decreased (Lis *et al.* 2008; Penna *et al.* 2010). This development has made it possible to investigate more catchments or events. Few early IHS studies compared different catchments (Rodhe 1987) and only recently has IHS been used to compare neighboring headwaters (Onda *et al.* 2006; Laudon *et al.* 2007) and/or many events (McGlynn *et al.* 2004; Lyon *et al.* 2008; James & Roulet 2009; Roa-García & Weiler 2010; Hrachowitz *et al.* 2011; Segura *et al.* 2012). Several of these runoff generation studies found a more variable event and pre-event water contribution, contrary to the presumed dominance in pre-event water found in the single headwater studies. Casper *et al.* (2003), Pellerin *et al.* (2008), Kienzler & Naef (2008), James & Roulet (2009), and Penna *et al.* (2014) could relate an increase of event water to rainfall sum, intensities, and duration (see also Klaus & McDonnell 2013). In forested headwaters, trees not only affect the amount of spatiotemporal throughfall (Gerrits *et al.* 2010) and isotopic composition (Allen *et al.* 2015), but also affect the subsurface connectivity (Weiler *et al.* 1998). Interception and transpiration of trees together with higher infiltration capacities of the soils can have a delaying effect on stream response, and pre-event water dominates the stormflow (Buttle 1994; Roa-García & Weiler 2010; Klaus & McDonnell 2013). Roa-García & Weiler (2010) observed higher pre-event water fractions in wetlands compared to forest and grasslands. Other studies have also observed higher event water fractions in wetlands (McCartney *et al.* 1998; Laudon *et al.* 2007) and in grasslands (Bonell *et al.* 1990). Infiltration capacity, soil type, storage potential of soils (Geris *et al.* 2015), and macropore distribution (Buttle 1994) are important controlling factors in runoff generation processes. High responsive headwaters with shallow soils of less than a meter have generally limited water storage in the soil mantel (Pearce 1990). Suecker *et al.* (2000) observed higher event water contributions on steep slopes. In different studies from around the world, described in Buttle (1994) or Jordan (1994), it is difficult to observe a relationship between event water contribution and geology. On the other hand, Onda *et al.* (2006) however did not observe a significant relation between soil depth and event water, but found that headwaters with 'permeable' geologies (larger number of cracks and fissures) had a lower event water contribution.

Brown *et al.* (1999) and Shanley *et al.* (2002) observed that event water contribution increases with catchment size, while no relation was found by either McGlynn *et al.* (2004) or James & Roulet (2009). Seasonality and the state of the system affect flow pathways (Hinton *et al.* 1994; Penna *et al.* 2014). Jordan (1994), Casper *et al.* (2003), and James & Roulet (2009) found that dry antecedent conditions with low connectivity result in higher event water contribution while McGlynn *et al.* (2004) found the opposite.

Pre-alpine headwaters are characterized by a large spatiotemporal variability of precipitation and variation in land cover, topography, and geology (Gurtz *et al.* 1999). Despite the heterogeneous catchment characteristics, baseflow processes in neighboring pre-alpine headwaters can be similar (Fischer *et al.* 2015). During stormflow however, it remains to be quantified how the variability of precipitation and catchment characteristics controls runoff processes in these headwaters.

In this study we investigated a steep pre-alpine region with high annual precipitation amounts (>2,000 mm y^{-1}) in Switzerland using IHS for five neighboring headwaters and 13 different rainstorm events. The objective was: (1) to assess differences in pre-event water contribution between headwaters and different events; and (2) to relate these differences to rainfall, catchment, and antecedent characteristics.

METHODS

Study area

The study area, the Zwäckentobel, is a pre-alpine catchment in Switzerland and approximately 40 km south of Zurich. The climate is humid with a mean annual temperature of 6 °C. The mean annual precipitation is 2,300 mm y^{-1}, of which half falls during the snow-free season (June–October). It rains approximately every second day and about one-third of the annual precipitation falls as snow (Stähli & Gustafsson 2006). The mean annual actual evaporation is approximately 300 mm y^{-1} (Menzel *et al.* 2007). The mountain streams respond quickly and can have high discharges

with large amounts of sediment transport (Turowski *et al.* 2009). After rainfall events, the streams return to baseflow within approximately 1 day.

The Zwäckentobel is a 4.3 km^2 south–north oriented headwater catchment. The east facing side of the catchment is steep with frequent landslides and an ephemeral stream network. Approximately 10 perennial streams drain the remaining part of the Zwäckentobel. One of the streams is the 0.7 km^2 Erlenbach catchment (WS04) which has been the subject of numerous studies since 1964 (Hegg *et al.* 2006). In 2009, the streams of WS07, WS10, WS11, and WS19 (0.09 to 0.21 km^2) were additionally gauged (Figure 1(a) and Table 1). Common features for all headwaters (WS04–WS19) are alternating steep slopes of more than 20 ° and flatter areas along the main axis, originating from erosion deposits like soil creep and landslides. The steep terrain and high transport capacity of streams created step-pool channels (Molnar *et al.* 2010) cutting into the alluvium of weathered bedrock (Keller 1970). As a consequence, a riparian zone is lacking (Hagedorn *et al.* 2001).

The geology of the Zwäckentobel has three different types of tertiary flysch: Wild, Waeggitaler, and Schlieren flysch. The different facies consist of different calcareous sedimentary layers of schist, marl or sandstone (Hantke 1967; Hsü & Briegel 1991) with creeping gleysols (0.5–2.5 m) on top (Figure 1(b)). The spatial distribution of shallow soils (depth ≤1 m) was taken from Fischer *et al.* (2015). The soils have a high silt and clay content resulting in a low matrix permeability but a high drainage capacity in macropores and the organic layer of 20–50 cm (Feyen *et al.* 1999).

The land cover of the Zwäckentobel was classified by Fischer *et al.* (2015) into forest, partly forested, meadows, and wetlands (Figure 1(c)). The dominant tree species in the Zwäckentobel is Norway spruce with a plate-shaped root network with an approximate root depth of 1 meter, in wet areas. Non-forested locations within the catchment are generally wetter and consist of bushed and/or swampy meadows or wetlands (Rinderer *et al.* 2012). During the summer months, meadows in the upper part (above 1,450 m) of WS04 and WS19 are used as alpine pastures.

Instrumentation

Precipitation was measured at 14 locations (Figure 1(a)). Two of the rain gauges are situated in the Erlenbach catchment (WS04) and have been measuring precipitation since 1964

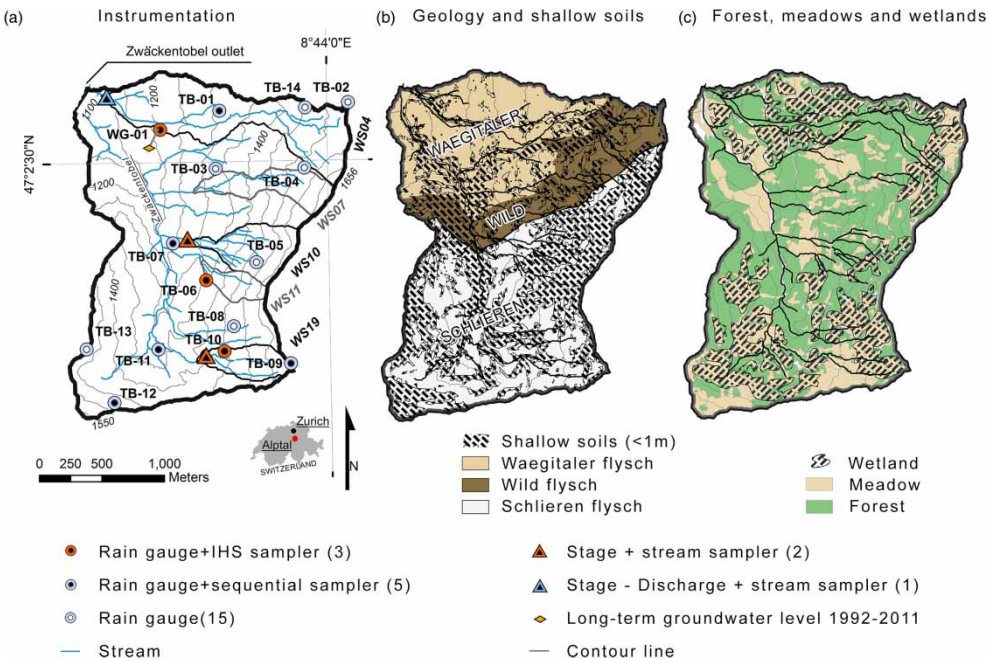

Figure 1 | Map of the Zwäckentobel: (a) sampling locations in selected headwaters WS04 to WS19; (b) geology: three different types of flysch and on top the shallow soils ≤1 m indicated as hatched areas; (c) land cover: forest and meadows with hatched areas indicating wetlands. Colour scheme of (b) and (c) adapted from www.ColorBrewer.org. Please refer to the online version of this paper to see this figure in colour: http://dx.doi.org/10.2166/nh.2016.176.

Table 1 | Catchment characteristics of the Zwäckentobel and its five headwaters

				ZT	WS04	WS7	WS10	WS11	WS19
Shape	Size		km^2	4.25	0.7	0.21	0.23	0.09	0.15
	Altitude	Max	m	1,656	1,656	1,656	1,598	1,583	1,598
		Mean		1,360	1,342	1,468	1,432	1,421	1,494
		Min		1,084	1,109	1,262	1,276	1,292	1,384
	Slope	Mean	°	19	17	21	23	24	18
		Max		56	49	47	53	45	43
Geology	Flysch	Waegitaler	%	29	64	16	0	0	0
		Wild		17	29	42	0	0	0
		Schlieren		54	7	42	100	100	100
	Soil depth	<1 m	%	29	44	55	73	74	49
Land cover	Forest		%	55	53	53	72	81	18
	Partly forested			21	22	27	14	10	1
	Meadow			24	25	20	14	9	81
	Wetland		%	29	33	28	23	21	51

(WG-01: Ott Pluvio, OTT Hydrometrie AG, Switzerland and TB-14: Joss-Tognini tipping bucket, Lamprecht meteo, Germany). The remaining 12 rain gauges (Davis II rain collector-tipping bucket; Davis Instruments Corp., USA with Odyssey data logger; Dataflow Systems, New Zealand) were distributed over the Zwäckentobel in the open field at a height of 1.5 m above ground level and measured rainfall during the period 2009–2011. Barometric pressure and air temperature were measured at WG-01 and WS19 (Keller DCX-22, Keller AG, Switzerland; Figure 1(a)).

In the Erlenbach catchment (WS04), stage/discharge has been measured with a concrete flume from 1984 to the present (Hegg *et al.* 2006). The headwaters WS07, WS10, WS11, and WS19 and the Zwäckentobel outlet (ZT) were gauged in 2009 (Keller DCX-22 pressure and temperature sensors, Keller AG, Switzerland, Figure 1(a)). Due to the frequently changing stream morphologies it was impossible to derive rating curves. In the vicinity of WG-01, groundwater levels have been measured since 1992 in a screened groundwater well and with an Ott-groundwater data logger (OTT Hydrometrie AG, Switzerland; Figure 1(a)).

Event sampling

In headwaters WS04, WS07, WS10, WS11, and WS19, different rainfall–runoff events were sampled during the snow-free season of 2010 and 2011 (Tables 2–4). Before each rainfall event, a grab sample was taken from each stream to determine the pre-event water composition. Rainwater samples for isotope analysis were collected with eight sequential rainfall samplers (adapted after Kennedy *et al.* (1979) containing 12×100 mL honey jars, each representing 5 mm of liquid precipitation, Figure 1(a)). At the catchment outlets of WS04, WS07, WS10, WS11, and WS19, automatic samplers collected streamwater samples (ISCO 6712 with 24×1 L bottles and Liquid Level Actuator, Teledyne Isco, USA; Figure 1(a)). The different automatic samplers started after the water level of the streams rose more than 1 cm and sampled six samples every 10 min during the rising limb, followed by 18 samples every 60 min. This sampling scheme allowed the rising limb to be sampled with a high temporal resolution, while taking at least one sample as close as possible to the maximum discharge peak, such as in event 2 (Figure 2, left). For large events, it was attempted to collect the water samples from the full automatic samplers. These samplers were reprogrammed and restarted (sampling interval 120 or 240 min) to capture parts of the falling limb of the hydrograph, such as in event 11 (Figure 2, right). To improve sample handling and avoid sample contamination (Wassenaar *et al.* 2014), we chose not to use mineral oil in rain and stream water sample bottles, and rather collected all samples directly after a rainfall event to

Table 2 | Hydrometeorological characteristics of the 13 sampled events

Event nr.	1	2	3	4	5	6	7	8	9	10	11	12	13
Year	2010				2011								
Day, month	8 Sep	17 Sep	24 Sep	4 Oct	29 Jun	8 Jul	14 Jul	15 Aug	24 Aug	27 Aug	4 Sep	18 Sep	6 Oct
A_{DS} [d]	7	1	5	2	3	5	1	2	3	0	0	1	14
A_{PI7} [mm]	2	50	6	10	24	5	41	23	2	10	9	26	0
A_{GL1} [cm]	−34	−23	−28	−19	−28	−36	−12	−28	−38	−41	−37	−23	−42
A_{Q1} [l s^{-1} km^{-2}]	7	16	3	7	10	7	11	7	1	4	0	13	1
P length [h]	10	8	70	10	23	11	30	37	2	19	11	11	33
P_{sum} [mm]	22 (2.6)	11 (1.4)	109 (16)	10 (1)	84 (19)	25 (1.5)	56 (17)	50 (15)	11.8 (2)	20.4 (1)	51 (11)	25 (2)	31(12)
P[mm h^{-1}]	2.2(0.3)	1.3 (0.2)	1.5 (0.2)	0.9 (0.1)	3.6 (0.9)	2.5 (0.2)	2 (0.6)	1.4 (0.4)	6 (1)	1 (0.1)	1.9 (0.4)	1.6 (0.2)	0.9 (0.4)
P_{max} [mm h^{-1}]	4.5 (0.6)	2.3 (0.3)	7.6 (1.1)	2.4 (0.4)	18 (8.4)	9 (0.9)	6.7 (1.6)	10 (2.7)	10 (3)	7.3 (0.7)	7 (1.4)	6 (1.4)	8.6 (3.5)
$H_{responds}$ [h]	0.6 (1)	1 (0.6)	0.2 (0)	0.3 (0.3)	0.2 (0.1)	0.1 (0.1)	0.3 (0.2)	0.7 (0.3)	0.1 (0.1)	0.4 (0.3)	0.3 (0.2)	0.3 (0.2)	1.3 (0.5)
Q_{peak} [l s^{-1} km^{-2}]	353	106	1,010	53	3,004	390	1,197	1,287	86	334	589	504	509
Q/P [-]	0.35	0.36	0.7	0.29	0.6	0.25	0.68	0.55	0.12	0.25	0.52	0.52	0.28

Antecedent dry spell (A_{DS}), antecedent precipitation index with 7 days prior to an event (A_{PI7}), antecedent groundwater level (A_{GL1}), antecedent discharge (A_{Q1}), rainfall duration (P length), mean event rainfall sum all rain gauges (P_{sum}), mean average hourly rainfall intensity of all rain gauges (P), maximum hourly rainfall intensity of all rain gauges (P_{max}), mean stream responds to rainfall of all headwaters (H responds), maximum specific discharge of WS04 (Q_{peak}), runoff coefficient (Q/P). Spatial standard deviation is in brackets.

Table 3 | For WS04–WS19 and events 1–13 the number of stream samples n_{Cs}, $\delta^{18}O$ [‰] of pre-event water *Cpe,* maximum and minimum event water *Ce* and maximum and minimum streamwater, IHS based minimum fraction of pre-event water f_{PE} and its corresponding uncertainty $W f_{PE}$. The letters np indicate events where an IHS was not possible

Event		1	2	3	4	5	6	7	8	9	10	11	12	13
Year		2010				2011								
Day, month		8 Sep	17 Sep	24 Sep	4 Oct	29 Jun	8 Jul	14 Jul	15 Aug	24 Aug	27 Aug	4 Sep	18 Sep	6 Oct
WS04	C_{pe}		−10.5	−10.4		−10.7	−8.45	−9.12	−8.5	−8.5	−8.51	−8.96	−9.01	−9.41
	$C_e - _{WG01}$		−4.6	−8.39		−4.61	−6.89	−6.89	−4.26	−2.9	−5.39	−3.15	−4.37	−8.89
			−6.63	−16.4		−9.35	−8.95	−8.95	−15.22	−5.27	−7.59	−13.33	−11.77	−10.47
	n_{Cs}		23	46		23	15	26	45	10	20	26	29	21
	C_s		−9.59	−10.4		−7.03	−8.67	−8.67	−8.76	−8.51	−8.08	−8.3	−8.01	−9.39
			−10.53	−12.94		−8.81	−9.73	−9.73	−10.32	−8.82	−9.23	−9.28	−9.07	−9.8
	f_{PE}		0.83	0.1		0.28	np	0.48	0.32	0.91	0.57	0.84	0.51	np
	$W f_{PE}$		±0.1	±0.87		±0.16		±0.3	±0.8	±0.35	±0.3	±0.16	±0.24	
WS07	C_{pe}	−10.64		−10.6		−9.39			−9.39				−9.49	−9.39
	n_{Cs}	24		49		34			9				24	20
	C_s	−8.84		−8.84		−8.84			−9.08				−8.31	−9.33
		−10.48		−10.48		−10.48			−10.13				−9.49	−9.85
	f_{PE}	np		0.1		0.61			np				np	0.29
	$W f_{PE}$			±0.87		±0.14								
WS10	C_{pe}	−10.64		−10.42	−10.7	−9.43		−9.35	−9.36	−10.24	−8.45	−8.95	−9.756	−9.73
	$C_e - _{TB06}$	−8.32		−8.87	−7.35	−4.61		−3.43	−3.75	−2.36	−4.96	−3.75	−4.64	−5.36
		−11.63		−20.4	−8.7	−9.35		−9.05	−14.19	−5.68	−7.52	−12.67	−11.88	−10.43
	n_{Cs}	24		53	24	35		7	6	8	10	20	23	24
	C_s	−10.35		−10.42	−10.27	−7.38		−7.86	−8.95	−8.4	−8.27	−8.17	−8.65	−9.19
		−10.79		−12.42	−10.88	−9.44		−9.82	−10.03	−10.24	−8.75	−9.52	−9.76	−10.19
	f_{PE}	np		0.36	0.84	0.55		0.42	np	0.67	0.84	np	0.6	np
	$W f_{PE}$			±0.34	±0.24	±0.16		±0.35		±0.15	±0.6		±0.19	
WS11	C_{pe}			−10.52				−9.964	−9.11	−10.5		−9	−9.89	−9.7
	n_{Cs}			54				15	15	20		23	18	24
	C_s			−10.16				−8.99	−8.95	−7.92		−8.35	−8.65	−9.16
				−12.29				−9.33	−9.85	−10.5		−9.33	−9.18	−10.18
	f_{PE}			0.49				np	np	0.6		0.86	0.57	0.74
	$W f_{PE}$			±0.25						±0.1		±0.17	±0.17	±0.29
WS19	C_{pe}	−10.46	−10.19	−10.26	−11.3	−9.1	−8.9						−8.79	−8.4
	$C_e - _{TB10}$	−8.13	−5.74	−8.88	−7.72	−5.3	−5.7						−4.75	−6.32
		−11.8	−7.87	−17.33	−9.06	−9.56	−9.66						−10.88	−12.14
	n_{Cs}	24	23	54	24	34	13						22	23
	C_s	−9.8	−8.92	−10.26	−10.35	−6.82	−8.55						−7.08	−8.71
		−11.04	−10.46	−14.32	−10.89	−8.54	−8.75						−8.8	−9.73
	f_{PE}	0.6	0.68	0.1	0.7	0.3	np						0.51	0.33
	$W f_{PE}$	±0.1	±0.13	±0.73	±0.1	±0.14							±0.4	±0.2

Table 4 | For WS04–WS19 and events 1–13 the number of stream samples n_{Cs}, δ^2H [‰] of pre-event water *Cpe*, maximum and minimum event water *Ce* and maximum and minimum streamwater, IHS based minimum fraction of pre-event water f_{PE} and its corresponding uncertainty $W f_{PE}$. The letters np indicate events where an IHS was not possible

Event		1	2	3	4	5	6	7	8	9	10	11	12	13
Year		2010				2011								
Day, month		8 Sep	17 Sep	24 Sep	4 Oct	29 Jun	8 Jul	14 Jul	15 Aug	24 Aug	27 Aug	4 Sep	18 Sep	6 Oct
WS04	C_{pe}		−66.8	−72.4		−68.7	−66.5	−62.1	−64.6	−57.1	−60.6	−59.8	−56.9	−61
	C_{e-WG01}		−26.1	−53.6		−25.4	−46.1	−21.8	−25.6	−19.7	−29.7	−17.3	−20.8	−60.3
			−45.1	−123.0		−64.1	−59.8	−52.6	−115.6	−24.9	−47.6	−96.0	−103.6	−73.2
	n_{Cs}		23	46		23	15	26	45	10	20	26	29	21
	C_s		−64.5	−71.2		−47.3	−57.6	−46.8	−59.7	−57.4	−53.8	−55.6	−52.9	−62.6
			−72.3	−92.4		−61.4	−66.5	−62.1	−73.6	−59.5	−62.4	−62.98	−61.0	−66.4
	f_{PE}		0.85	0.1		0.34	np	0.51	0.26	0.65	0.65	0.9	0.52	np
	$W f_{PE}$		±0.12	±0.88		±0.17		±0.26	±0.9	±0.35	±0.34	±0.2	±0.24	
WS07	C_{pe}	−71		−73.2		−58.7			−64.6				−60.9	−60.9
	n_{Cs}	24		49		34			9				24	20
	C_s	−69.8		−72.5		−51.4			−62.4				−54.9	−62.4
		−74.2		−90.6		−62.6			−69.6				−64.4	−67.4
	f_{PE}	np		0.1		0.72			np				np	0.29
	$W f_{PE}$			±0.8		±0.18								
WS10	C_{pe}	−73.8		−72.3	−71.3	−72.1		−68.5	−64.6	−70.9	−57.5	−63.3	−60.9	−66.7
	C_{e-TB06}	−54.1		−29	−55.1	−49.5		−29.3	−20.3	−18.3	−28.1	−23.2	−23.8	−32.8
		−77.8		−34.4	−153.7	−62.9		−60.9	−107.7	−27.9	−45.7	−89.6	−82.6	−68.8
	n_{Cs}	24		53	24	35		7	6	8	10	20	23	24
	C_s	−69.9												
		−71.3	−71.1	−47.5		−51.6	−62.4	−54.5	−55.2	−56.1	−64.2	−60.6		
		−75.1		−89.1	−74.7	−63.8		−68.5	−69.3	−70.9	−58.9	−64.2	−57.1	−63.8
	f_{PE}	np		0.32	0.9	0.55		0.39	np	0.66	0.84	np	0.59	np
	$W f_{PE}$			±0.58	±0.37	±0.16		±0.36		±0.1	±0.39		±0.19	
WS11	C_{pe}			−72.2				−62.2	−64.6	−72.1		−58.3	−57.6	−60.3
	n_{Cs}			54				15	15	20		23	18	24
	C_s			−70.8				−60.9	−65	−48.3		−55.7	−57.1	−60.8
				−88.5				−64.1	−68.7	−72.1		−63.4	−67.7	−69.8
	f_{PE}			0.36				np	np	0.55		0.8	0.57	0.74
	$W f_{PE}$			±0.53						±0.1		±0.28	±0.17	±0.29
WS19	C_{pe}	−69.8	−69.4	−70.2	−74.9	−47.2	−66.5						−46.6	−57.5
	C_{e-TB10}	−50.7	−33.6	−55.3	−50.3	−31	−15						−23.9	−39.2
		−77.1	−49.4	−127.9	−63.9	−67.6	−61.8						−70.2	−82.5
	n_{Cs}	24	23	54	24	34	13						22	23
	C_s	−67.7	−60.7	−69.9	−71.8	−42.6	−55.9						−46.7	−57.8
		−72.8	−71.7	−104.3	−75.4	−57.3	−58.7						−60.1	−65.9
	f_{PE}	0.68	0.75	0.1	0.87	0.6	np						0.47	0.33
	$W f_{PE}$	±0.1	±0.14	±0.8	±0.27	±0.35							±0.15	±0.2

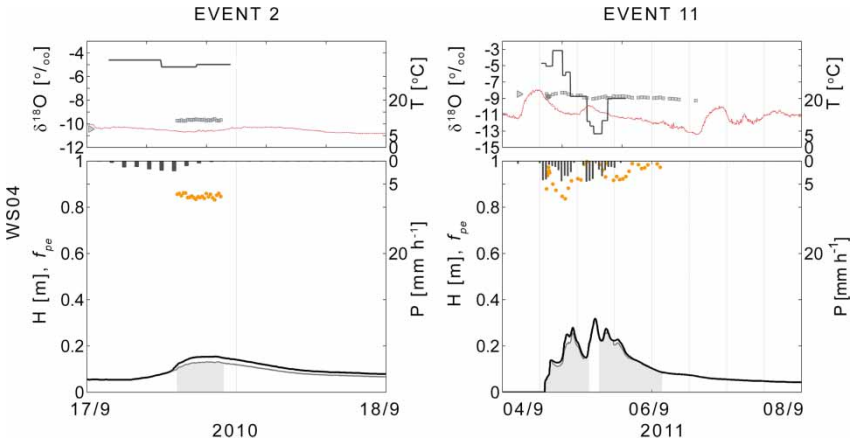

Figure 2 | For WS04, sampled events 2 and 11. The top panels show the $\delta^{18}O$ in event water (dark line), streamwater (grey squares), pre-event water (triangle), and air temperature (dashed line). Bottom panels show precipitation (inverted, from the top), water level (solid dark line), and fraction of pre-event water *fpe* (circles and grey area below the hydrograph).

prevent fractionation. In the field, rainfall and stream samples were filled in a 20 mL glass for transport and storage (20 mL glass with cap and additional Teflon/rubber septum). Excess water from all sampler tubing, bottles, and tipping buckets was removed, i.e., dried as well as possible to prevent inter-event contamination. Due to malfunctioning of some automatic samplers (e.g., air bubbles or sediment in the water level actuators or power failures when temperatures fell below 5 °C), not all events were sampled equally for all streams. The number of water samples for stable isotope analysis per stream and event ranged from seven samples (short events) up to 54 samples (for long events). The number of sampled events varied per stream from 6 to 11 (Table 3).

Water sample analysis

The collected water samples were analyzed for their stable isotope composition at the stable isotope laboratory of the University of Zurich, Department of Geography. All water samples were filtered (0.45 µm filter 25 mm PTFE Syringe Filter, Simplepure USA) and pipetted in a vial (1 mL into a 1.5 mL 32 × 11.6 mm screw neck vials with cap and PTFE/silicone/PTFE septa) prior to analysis. Samples were analyzed with a Cavity Ring-Down Spectroscope-Picarro L1102-i Liquid Analyser (1st generation analyser, Picarro Inc. 2008). The analysis scheme of Penna *et al.* (2010) was followed, and values were reported as δ-values in per mille (‰) relative to Vienna Standard Mean Ocean Water. Most samples could be measured with a precision for δ^2H of <0.5‰ and for $\delta^{18}O$ of <0.1‰. Due to some technical issues with the spectroscope, for some samples the accuracy for δ^2H was >1‰ while for $\delta^{18}O$ it remained <0.1‰.

IHS

For the different rainfall–runoff events a IHS was used to quantify the fraction of pre-event water in storm runoff, f_{PE} (Equations (1) and (2)) (Sklash & Farvolden 1979):

$$Q_s = Q_E + Q_{PE} \tag{1}$$

$$f_{PE} = \frac{C_S - C_E}{C_{PE} - C_E} \tag{2}$$

The symbol C describes the stable isotope composition of stormflow (streamwater), baseflow (pre-event water), and rainfall (event water) indicated with subscripts *S*, *PE*, and *E*, respectively. The incremental intensity mean (McDonnell *et al.* 1990) was used to account for the event water (Equation (3)). Here, I_i is the rainfall intensity and δ_i is the stable isotope composition of the accompanying precipitation. Some sequential rainfall samplers malfunctioned during some events. Therefore the nearest sequential rainfall sampler, which sampled the majority of the events, was assigned to each headwater (WG-1 for WS04 and WS07, TB-6 for WS10 and WS11, and TB-10 for WS19) to be

used in the IHS.

$$C_E = \frac{\sum_{i=1}^{n} I_i \delta_i}{\sum_{i=1}^{n} I_i} \quad (3)$$

For each of the 13 events, the uncertainty of the pre-event water contributions was quantified based on Equation (4) (Genereux 1998) with a confidence level of 0.05. The symbols $W_{f_{PE}}$, f_{PE}, and f_E represent the uncertainty in the pre-event water, and the fraction of pre-event and event water, respectively. W_{CE} is the uncertainty in event water and estimated using the standard deviation of the collected stable isotope composition of the nearest sequential rainfall sampler. A data set that had been collected during a previous baseflow snapshot campaign by Fischer *et al.* (2015) was used to quantify the uncertainty of pre-event water W_{CP}. For each headwater catchment the baseflow samples within the catchment were used to calculate the standard deviation of the stable isotope composition. Streamwater uncertainty, W_{CS}, was based on the laboratory precision of repeat measurements:

$$W_{f_{PE}} = \left\{ \left[\frac{f_E}{(C_E - C_{PE})} W_{CE} \right]^2 + \left[\frac{f_{PE}}{(C_E - C_{PE})} W_{CPE} \right]^2 + \left[\frac{-1}{(C_E - C_{PE})} W_{CS} \right]^2 \right\}^{1/2} \quad (4)$$

Data analysis

For each sampled event, three proxies were used to describe the antecedent conditions of the study area (Table 2). Based on rain gauge WG-01 (1998–2011), the antecedent precipitation index, with 7 days prior to an event (A_{PI7}), was calculated. Additionally, the antecedent discharge (A_{Q1}; WS04) and groundwater level (A_{GL1}; long-term groundwater well near WG-01) were derived, both for 1 day prior to an event. From 14 rain gauges, the mean and standard deviation of different rainfall characteristics were derived for each event. In WS04, the maximum discharge Q_{max} was derived and the runoff coefficient was additionally computed by subtracting the baseflow from the total stormflow divided by the event rainfall sum, analogous to Burch *et al.* (1996). Baseflow was defined as a straight line from the rise of the hydrograph to the inflection point where the hydrograph in the semi-logarithmic domain flattens. For every event, the exceedance probabilities of maximum event discharge (WS04, 1998–2011) and event rainfall sum (WG-1, 1998–2011) were determined (Figure 3).

In addition to standard representation of the IHS (hydrograph, precipitation, air temperature, stable isotope, and calculated pre-event water), we related the rainfall characteristics, antecedent conditions, and baseflow, 1 day before an event (WS04), to the observed minimum f_{PE} (near the maximum discharge) using a linear relation to explain differences in pre-event water. Additionally, five types of multiple linear regression were performed, where for each type, the rainfall characteristics, antecedent conditions, and baseflow 1 day before an event (WS04), were added stepwise to relate to the observed minimum f_{PE} to explain differences in pre-event water.

RESULTS

Sampled event characterization

Thirteen rainfall–runoff events were sampled during the snow-free seasons of 2010 and 2011 (see Table 2). The

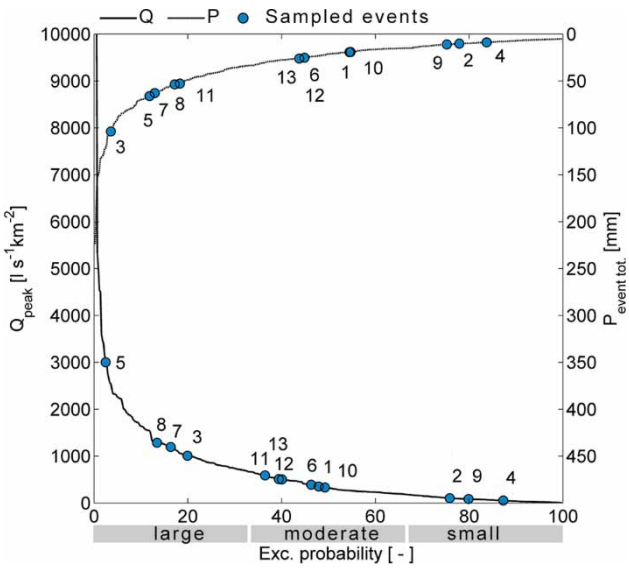

Figure 3 | Peakflow exceedance curve (WS04, Q_{peak} >33 l s^{-1} km^{-2}), event rainfall sum distribution (WG-01, P_{sum} >5 mm) for the period 1998–201,1 and where circles indicate the sampled events 1–13.

events covered a wide range of different rainfall and peak discharge magnitudes observed during the time period 1998–2011 (Figure 3). The mean hourly rainfall intensities of all rain gauges of the Zwäckentobel varied between 1 and 6 mm h^{-1} with a maximum of up to 18 mm h^{-1} and a large spatial variability (Table 2). The discharge of WS04–WS19 responded to rainfall with a delay of 10 min up to 1 hour for the different events (Table 2). Each of the events had different antecedent wetness conditions with A_{PI7} ranging from wet to dry (Figure 4). The baseflow 1 day before an event (A_{Q1}) was below 0.1 up to 16 l s^{-1} km^{-2}. The groundwater levels before an event (A_{GL1}) were between −12 and −42 cm below ground surface.

Stable isotopes and hydrograph separation of sampled storm events

The isotopic composition of all isotope water samples followed the global meteoric water line (GMWL) and no fractionation was observed (Figure 5(a)). The IHS was performed using both δ^2H and $\delta^{18}O$, which mainly resulted in 60 similar pre-event fractions with only two exceptions: WS04 event 9 and WS19 event 5 (Tables 3 and 4, and Figure 5(b)). Since both isotopes resulted in rather similar computed pre-event water contributions, only the computations based on $\delta^{18}O$ are shown in the following.

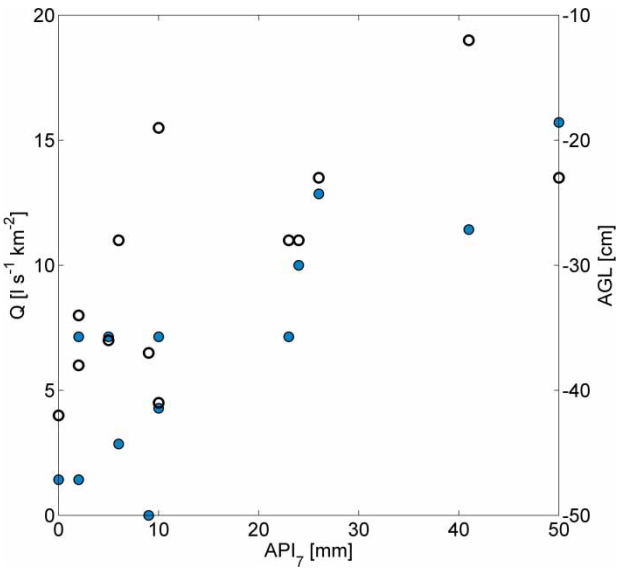

Figure 4 | Antecedent discharge (closed circles) and antecedent groundwater level (open circles) against antecedent precipitation index for the sampled events 1–13.

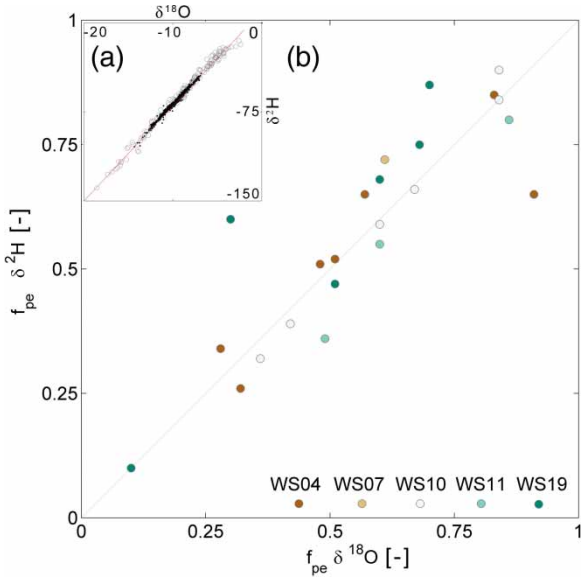

Figure 5 | (a) Inset: all collected rainfall samples (grey circles) and stream samples (black circles) of all headwaters and events follow the global meteoric water line. (b) Values of the minimum fraction of pre-event water computed based on $\delta^{18}O$ observations versus the corresponding values that were computed based on δ^2H observations for the different events and catchments (each catchment is represented by a different colour). The grey line is where pre-event water computations based on $\delta^{18}O$ and δ^2H observations would be equal. Please refer to the online version of this paper to see this figure in colour: http://dx.doi.org/10.2166/nh.2016.176.

The $\delta^{18}O$ in pre-event water varied for the different streams and the different events by 0.5–1‰ (Table 3 and Figure 6). The $\delta^{18}O$ in event water varied for the different sampling locations by 0.5 and 2‰ and the temporal variability of events was 2 up to 12‰ (Table 3 and Figure 6). The $\delta^{18}O$ difference between pre-event water and streamwater samples near the peak was about 0.5–2‰ and up to 0.5–4‰ for some larger events (Table 3 and Figure 6).

The minimum fraction of pre-event water (f_{PE}) for the different streams and events varied from 0.01 up to 0.9 and occurred half an hour before or after a maximum water level (Figure 6). For some events, the rainfall, pre-event, or streamwater sample compositions were too similar to allow the fraction of pre-event water to be calculated (Table 3). In events where IHS was possible, the uncertainties in the minimum fraction of pre-event water (Wf_{PE}) were between ±0.1 up to ±0.9 (Table 3).

Comparison of three headwaters and events

The three headwater catchments with the best data coverage (WS04, WS10, and WS19) were selected for a more detailed

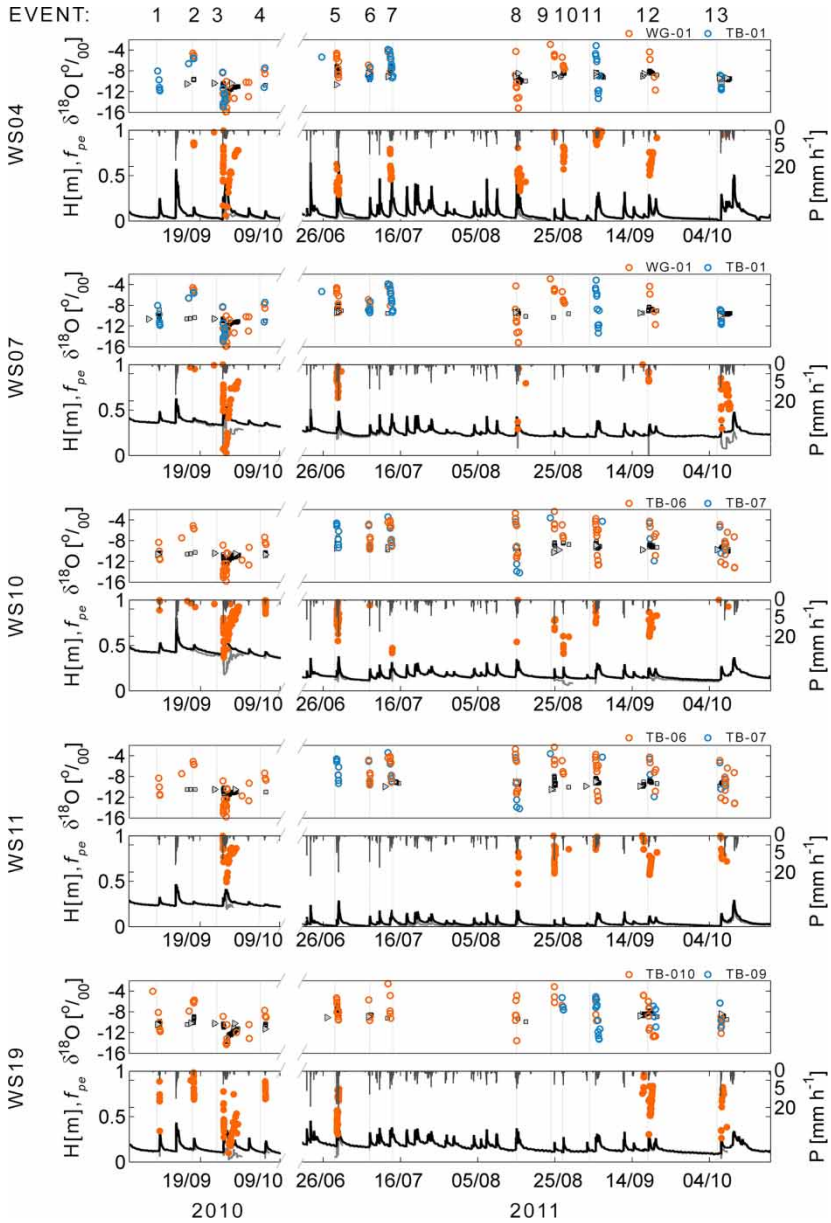

Figure 6 | Hydrometric and $\delta^{18}O$ overview of WS04–W19 and events 1–13. The top panels show $\delta^{18}O$ in event water (open circles and colours indicate different rain gauges), streamwater (grey squares) and pre-event water (triangle). Bottom panels show precipitation (inverted, from the top), water level (solid dark line), and fraction of pre-event water f_{pe} (circles). Please refer to the online version of this paper to see this figure in colour: http://dx.doi.org/10.2166/nh.2016.176.

comparison. In event 3, the maximum event rainfall sum was recorded above WS10, while different rainfall gradients were observed in WS04 and WS19 (Figure 7(a) and 7(d)). The rainfall intensities were moderate and spatially equal (Table 2 and Figure 7(a)) and the hydrograph had multiple peaks (Figure 8, left column). After the maximum water level was reached, the air temperature decreased to 0 °C, and the rainfall changed to snowfall. The $\delta^{18}O$ in event water of sampler WG-1, TB-6, and TB-10 started with a similar value but decreased to different minimums (Table 3 and Figure 8, left column). During the rain-free period after the first peak, streamwater samples were missing because the automatic water samplers were full. Shortly before the maximum water level, all samplers were restarted twice. The $\delta^{18}O$ in pre-event water and streamwater were similar for WS04 and WS10 while for WS19 it was slightly more

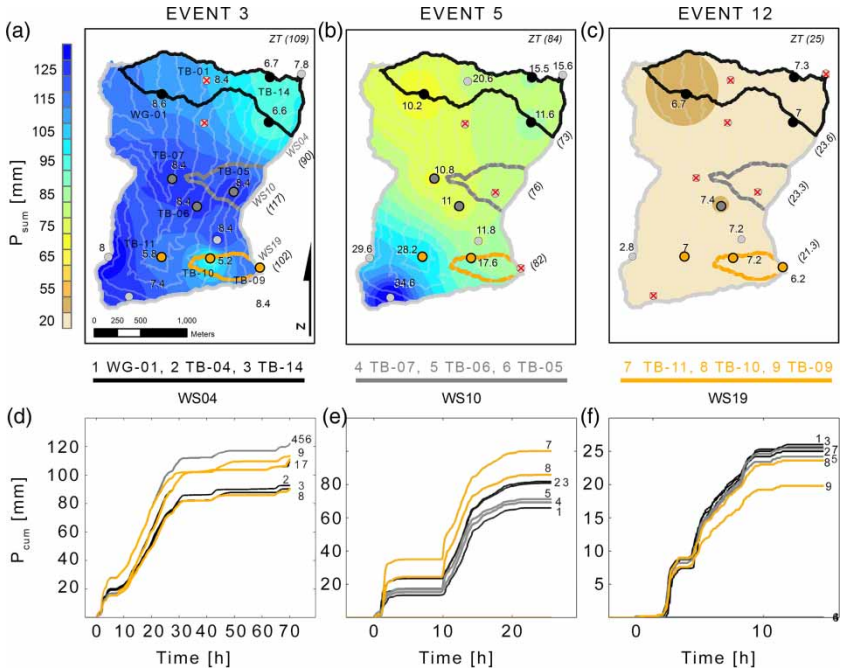

Figure 7 | Spatial distribution of event rainfall [mm] for (a) event 3, (b) event 5, and (c) event 12. Circles indicate rain gauges where text indicates the maximum event rainfall intensity [mm h^{-1}]. The headwater areal event rainfall [mm] is listed in brackets. Crosses indicate technical failures of rain gauges or sequential samplers. (d), (e), and (f) indicate the accumulated event rainfall [mm] of the different rain gauges in WS04, WS10, and WS19.

depleted (Table 3 and Figure 8, left column). The fraction of pre-event water decreased rapidly after the start of rainfall to a minimum of 0.2, 0.36, and 0.27, respectively (Figure 8, left column). During the second peak, WS04 and WS19 had dominant event water, while WS10 had a higher fraction of pre-event water. During the recession of the hydrograph, the fraction of pre-event water rose irregularly due to short additional rainfall that instantaneously increased the fraction of event water.

In event 5, the rainfall amount and intensities increased from WS04 towards WS19 (Table 2 and Figure 7(b) and 7(e)) and the hydrograph had two peaks (Figure 8, middle column). The $\delta^{18}O$ in event water of sampler WG-1 and TB-6 had a similar range, but were temporally different, while TB-10 was more depleted (Table 3 and Figure 8, middle column). The $\delta^{18}O$ in pre-event water and streamwater samples in WS04 and WS10 were alike and became more enriched towards the first peak of the hydrograph, while WS19 was more depleted. In all streams, the fraction of pre-event water decreased rapidly towards the first peak and increased during the intra-event of 6 hours. With the onset of the rain, the streams responded fast and WS04 had the highest recorded discharge of the 13 events sampled (Figure 2). The fraction of pre-event water was 0.3 for WS04 and WS19, during the first and second peak. In WS10, the fraction of pre-event water during the first peak was 0.72 and decreased during the second peak to 0.55. After the maximum water level the different automatic water samplers were full, and were not restarted, and therefore further observations were missing.

Event 12 had an average and evenly distributed event rainfall sum and intensity (Table 2 and Figure 7(c) and 7(f)) and the hydrograph had multiple peaks (Figure 8, right column). The $\delta^{18}O$ in event water of sampler WG-1 and TB-10 were alike, while more depleted in TB-06 (Table 3 and Figure 8, right column). The $\delta^{18}O$ in pre-event water in WS04, WS10, and WS19 were alike and the streamwater increased on average 1‰ during events. The rising limb was not sampled due to technical problems and started just at the maximum water level. The three different headwaters had fractions of pre-event water ranging from 0.51 to 0.6 and increased gradually during the falling limb to 1 (Table 3 and Figure 8, right column).

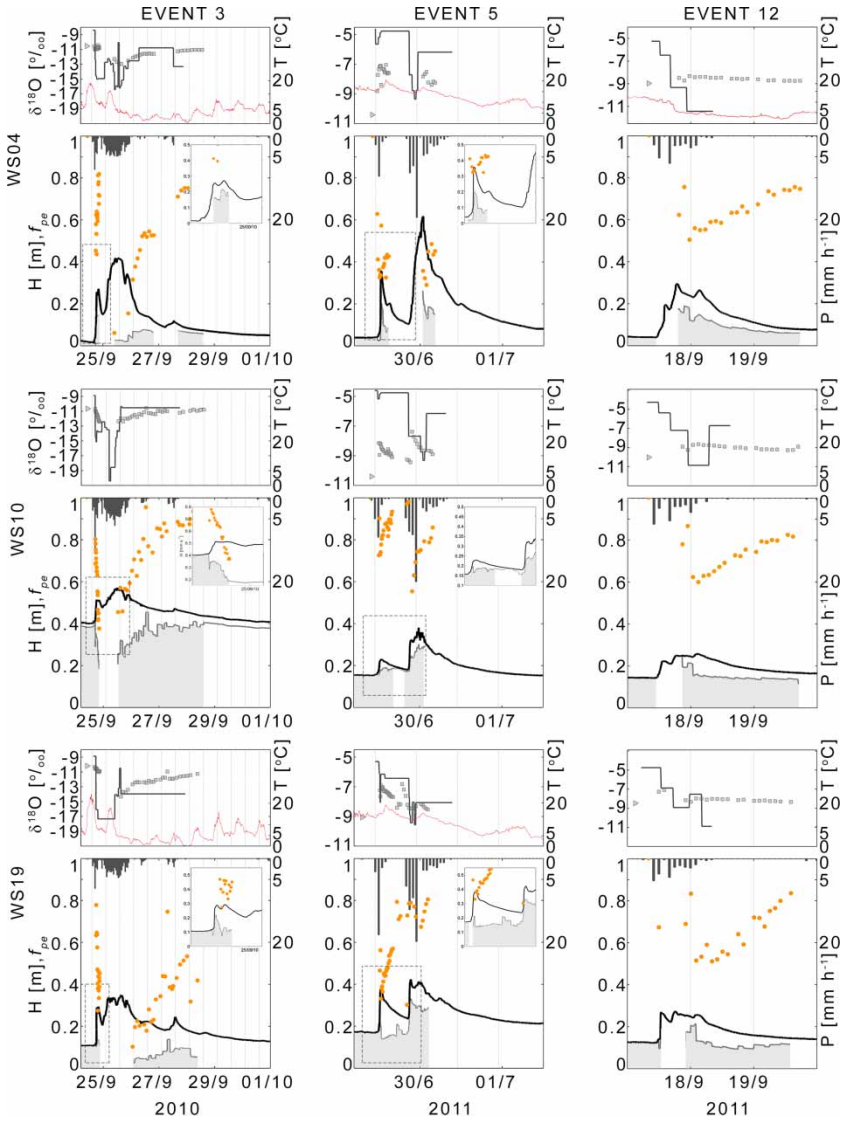

Figure 8 | Detailed hydrometric and $\delta^{18}O$ overview of headwaters WS04, WS10, and W19 and event 3, 5, and 12. The top panels show $\delta^{18}O$ in event water (line), streamwater (grey squares), pre-event water (triangle), and air temperature (dashed line). Bottom panels show precipitation (inverted, from the top), water level (solid dark line), and fraction of pre-event water f_{pe} (circles and grey area below the hydrograph).

Explanatory factors of pre-event water fractions

In WS04, WS10, and WS19 the minimum fraction of pre-event water decreased with increasing event rainfall sum (Figure 9, left column). To a lesser extent, the minimum fraction of pre-event water decreased with increasing maximum hourly rainfall intensities (Figure 9, right column). For both WS04 and WS19, the fraction of pre-event water in events 3, 5 and 12 was lower compared with WS10 (Figure 9). In addition, no relation between antecedent wetness and minimum fraction of pre-event water was observed (Figure 9). The relation between the minimum fractions of pre-event water was supported by the regression analysis. The rainfall sum correlated best with the minimum fraction of pre-event water in studied headwaters and for the individual headwaters (Table 5). Rainfall intensity correlated less with the minimum fraction of pre-event water and added little information in combination with rainfall sum to explain the pre-event water. The antecedent wetness indices A_{PI7}, A_{GL1}, and A_{Q1} correlated only weakly with the

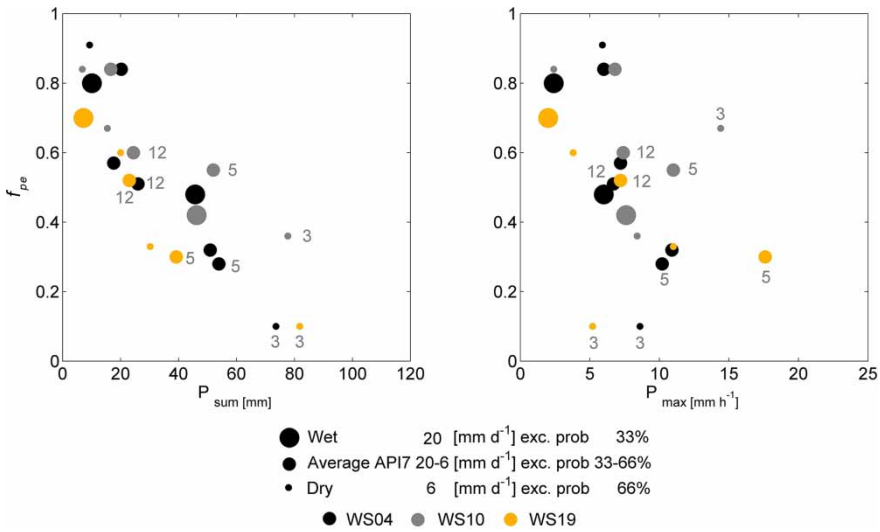

Figure 9 | The event rainfall sum related to the minimum fraction of pre-event water f_{pe} (left) and max rainfall intensity related to the minimum fraction of pre-event water *fpe* (right) for WS04, WS10, and WS19. Different sizes of circles indicate different antecedent conditions (wet, average, and dry) and numbers refer to events 3, 5, and 12.

Table 5 | Multiple linear relation of pre-event water and different predictors

	R^2	F	p
WS04, WS07, WS10, WS11, WS19			
$f_{PE\ min} = 0.80–0.01\ P_{sum}$	0.50	30	<0.001
$f_{PE\ min} = 0.71–0.02\ P_{max}$	0.13	4.25	0.04
$f_{PE\ min} = 0.43–0.06\ A_{PI7}$	0.03	1.1	0.3
$f_{PE\ min} = 0.42–0.004\ A_{GL1}$	0.02	0.7	0.4
$f_{PE\ min} = 0.52–0.003\ A_{Q1}$	0.002	6.2	0.02
$f_{PE\ min} = 0.91–0.01\ P_{sum}–0.02\ P_{max}$	0.53	16.2	<0.001
$f_{PE\ min} = 0.91–0.01\ P_{sum}–0.02\ P_{max}–0.004\ A_{PI7}$	0.53	10.4	<0.001
$f_{PE\ min} = 0.91–0.01\ P_{sum}–0.02\ P_{max}–0.004\ A_{PI7} + 0.001A_{GL1}$	0.58	9.3	<0.001
$f_{PE\ min} = 0.87–0.01\ P_{sum}–0.02\ P_{max}–0.001\ A_{PI7} + 0.004A_{GL1}–0.002A_{Q1}$	0.64	8.9	<0.001
WS04 $f_{PE\ min} = 0.92–0.01\ P_{sum}$	0.87	49.9	<0.001
$f_{PE\ min} = 0.99–0.01\ P_{sum}–0.01\ P_{max}$	0.88	24.7	<0.001
WS07 $f_{PE\ min} = 1.1–0.01\ P_{sum}$	np		
$f_{PE\ min} = 1.1–0.01\ P_{sum}\ {}_{+}0.01\ P_{max}$	np		
WS10 $f_{PE\ min} = 0.83–0.01\ P_{sum}$	0.80	20.2	<0.001
$f_{PE\ min} = 0.88–0.001\ P_{sum}–0.01\ P_{max}$	0.82	9.07	<0.1
WS11 $f_{PE\ min} = 0.8–0.003\ P_{sum}$	0.02	0.04	0.85
$f_{PE\ min} = 0.85–0.003\ P_{sum}–0.001\ P_{max}$	0.02	0.01	0.98
WS19 $f_{PE\ min} = 0.73–0.01\ P_{sum}$	0.94	65	<0.001
$f_{PE\ min} = 0.78–0.001\ P_{sum}–0.02\ P_{max}$	0.99	>100	<0.001

Minimum fraction of pre-event water ($f_{PE\ min}$), event rainfall sum (P_{sum}), maximum hourly rainfall intensity (P_{max}), antecedent precipitation index with 7 days prior to an event (A_{PI7}), antecedent groundwater level (A_{GL1}), antecedent discharge (A_{Q1}) of WS04.

minimum pre-event fraction. No significant relation between pre-event water and different catchment characteristics was found (analysis not shown).

The runoff coefficient was only available in WS04 and examined for temporal changes in relation to event rainfall sums (Figure 10). For events with rainfall sums less than 50 mm, the runoff coefficient was below 0.5 (Figure 10). With increasing event rainfall sum, the runoff coefficient increased to 0.7 (P = 110 mm), while the fraction of pre-event water decreased to 0.1. The overall pattern of the runoff coefficient in relation to event rainfall sums resembled the power law relation defined by Burch *et al.* (1996) (Figure 10).

DISCUSSION

Assessment of pre-event water contribution

In our studied headwaters, we observed large spatial variability in rainfall sum, intensity, and stable isotope composition for the large events, over relatively short distances (100 m). The spatiotemporal variability of $\delta^{18}O$ in event water was larger compared to the spatial variability

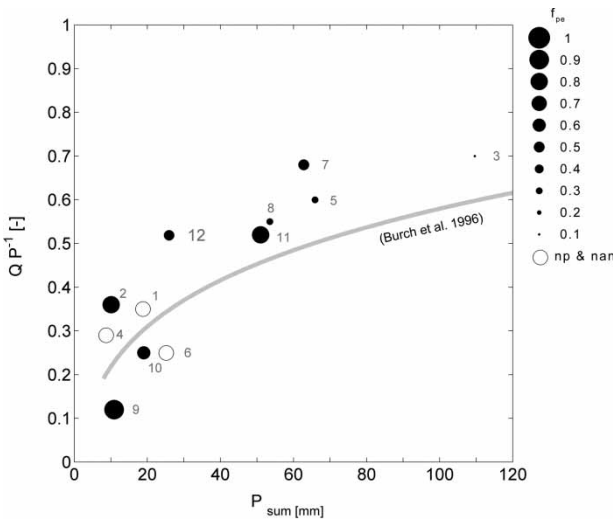

Figure 10 | The runoff coefficient for catchment WS04 as a function of the event rainfall sum (WG-01). The line illustrates the Burch *et al.* (1996) derived relation between runoff coefficient and event rainfall sum. Each circle indicates one of the 12 events of this study. The circle size of closed circles indicates the minimum fraction of pre-event water of WS04. Open circles refer to events where IHS was not possible or isotope data were not sampled.

of $\delta^{18}O$ in pre-event water and streamwater samples. These observations support the idea that small forested headwaters are often erroneously assumed to have homogeneous rainfall patterns (Goodrich *et al.* 1995) and isotopic compositions of precipitation (Lyon *et al.* 2008; Holko *et al.* 2012). Lyon *et al.* (2009) found that the spatial and temporal variability of the isotope composition may result in different fractions of pre-event water, depending on the use of $\delta^{18}O$ or $\delta^{2}H$ in the IHS. In this study, however, the differences between fractions of pre-event water computed based on $\delta^{18}O$ and $\delta^{2}H$ were smaller (±10%) compared to the large difference reported by Lyon *et al.* (2009). Furthermore, the differences in fraction of pre-event water using $\delta^{18}O$ or $\delta^{2}H$ were generally smaller than the IHS error propagation estimates. The large uncertainties were the result of, as Genereux (1998) suggested, small differences in $\delta^{18}O$ between event water and pre-event water. Large differences in $\delta^{18}O$ between event and pre-event isotopic composition are generally expected in summer months and therefore summer is considered as the favorable season to perform an IHS (Vitvar & Balderer 1997). This benefit however, was not always so strong for the 13 studied events and an IHS was not always possible. This could have been caused by the altitude of the studied headwaters above 1,100 m. This altitude resulted in a temperature decrease towards 0 °C with snowfall, even during summer, for certain events. The lower temperatures resulted in a more depleted isotopic composition compared to the average seasonal isotopic compositions. With high soil surface temperatures, the snow melted immediately and contributed to runoff generation. Late summer events, such as event 3 or 13, had lower air temperatures and the snow cover persisted, acting as an extra storage of precipitation. As a consequence, the stormflow magnitude in relation to its rainfall sum decreased. During snowmelt no fractionation was observed in stream samples. However, we cannot exclude that fractionated melt water was diluted by pre-event water, or that snow melt contributed to delayed stream flow.

The isotope composition of rainfall was sampled with a higher resolution compared to many other studies (e.g., sampling locations, temporal resolution, and events). Nonetheless, due to the observed spatial variability of stable isotopes in precipitation and stream samples, using the nearest rain gauge for each headwater in the IHS might have

introduced an incomplete accounting of event water in space and time, as described by Buttle (1994). This might have been the case for large events with large spatial gradients of rainfall amounts, intensities, and stable isotopes. Furthermore, forest interception and throughfall can result in changed isotopic signatures (Saxena 1987; Allen *et al.* 2015). Since the rainfall was sampled only in the open field this might have influenced the IHS results. Despite the incomplete sampling of rainfall and uncertainties in the fraction of pre-event water, the general pattern of fast response and recession of the hydrograph, and fraction of pre-event water, were analogous with plot scale tracer experiments by Feyen *et al.* (1999) and Weiler *et al.* (1998, 1999) and two events described by Weiler *et al.* (1999). Our study observed a high variability in fraction of pre-event water between the different events, which is opposite to the perception that humid-forested headwaters have dominant pre-event water during the peak discharge (Buttle 1994). This underlines the idea that when neglecting the spatial and temporal variability of rainfall characteristics and isotopic composition, one might get an incomplete picture of runoff processes.

Rainfall as a dominant factor in runoff processes

The frequent rainfall marked the headwater's wet character and its spatiotemporal dynamic. The fast hydraulic response of the streams and decrease of the fraction of pre-event water indicated the strong connection between rainfall and runoff. A statistical evaluation of controlling mechanisms was not possible because of the irregularly sampled data set (due to technical and logistic constraints). Instead, the minimum fraction of pre-event water was available for most sampled events. Buttle (1994) used the minimum fraction of pre-event water to compare different studies around the world and concluded that pre-event water dominated the peak discharges. Similarly, the minimum fraction of pre-event water was used in our study watersheds to compare processes that occur during the peak discharge. Despite the uncertainty, the minimum fraction of pre-event water, used as a qualitative proxy, indicated the overall pre-event or event water contribution during stormflow and could be related to explanatory variables. Rodhe (1987) found a decreasing relation of fraction of pre-event water with increasing snowmelt (for six headwaters distributed throughout Sweden with 2–6 snowmelt events per headwater). A similar decreasing relation of the fraction of pre-event water with increasing rainfall sums was observed for plot scale experiments (Weiler *et al.* 1999; Kienzler & Naef 2008), in a single urban catchment (Pellerin *et al.* 2008), and in a single pre-alpine headwater (Penna *et al.* 2014). Our study confirmed this relation and proved the validity in neighboring headwaters with different catchment characteristics (WS04–WS19). Renshaw *et al.* (2003) instead described a positive relation of the fraction of pre-event water with increasing precipitation, which might be caused by the smaller event rainfall sums and resulted in dominant pre-event water contribution. Considering all sampled events of WS04–WS19, the minimum fraction of pre-event water largely depended on the rainfall sum and, to a smaller degree, on the rainfall intensity. For individual streams the relation of minimum fraction of pre-event water and rainfall sum was even stronger. In WS07 and WS11, the fewer possible IHS did not allow for a statistical analysis. However, it is likely that in these headwaters the rainfall sum would also be a strongest predictor. The strong relation of rainfall sum and the fraction of pre-event water together with the spatial distribution of rainfall explained to a large degree the differences in pre-event water of WS04-WS19.

Compared to Blume *et al.* (2007), the error made by separating the hydrograph of WS04 into fast flow and baseflow was small due to the clear difference in antecedent baseflow and higher (by orders of magnitudes) stormflow. The runoff coefficient of the different sampled events in WS04 was also similar to the power law defined by Burch *et al.* (1996). Separating the runoff into fast flow and baseflow is extensively criticized (Klaus & McDonnell 2013), since it does not represent the observed dominant pre-event water contribution in forest headwaters (Buttle 1994; McGlynn *et al.* 2002). However, the combination of the runoff coefficient with the minimum pre-event water contribution, provides additional useful information. Instead of separating the hydrograph into fast and slow runoff processes, the runoff coefficient described the volume of discharge produced due to a certain amount of precipitation. In combination with the IHS, it became visible that the volume of discharge contained a certain fraction of event water and both similarly increased with increasing precipitation.

Catchment characteristics as secondary factors in runoff processes

The observed variable fraction of pre-event water in WS04-WS19 was different compared to the more stable observations made in catchments with a similarly high annual precipitation amount (>2,000 mm y^{-1}) such as the Maimai (McGlynn *et al.* 2002) or H. J. Andrews catchment (McGuire & McDonnell 2010). The differences in fraction of pre-event water might be due to the differences in land cover. The Maimai and H. J. Andrews catchment are predominantly forested compared to the mixed land cover (meadows, forests, and large percentage of wetlands 20–50%) of the Zwäckentobel. A higher pre-event water contribution was observed in stormflow of forested catchments compared to wetlands (McCartney *et al.* 1998; Laudon *et al.* 2007) or grasslands (Bonell *et al.* 1990). Plot scale experiments found differences in runoff processes for different soils (Feyen *et al.* 1999) and land covers (Weiler *et al.* 1998). However, no strong relation between the fraction of pre-event water and land cover could be noticed when comparing WS04–WS19 with each other. A small influence of land cover on runoff processes was noticeable for only some events. In WS10 and WS11 (steeper slopes, shallow soils, smaller amount of wetland, and large forested areas), for the larger events, a slightly higher pre-event water contribution and additional weaker relation of pre-event water with rainfall was observed compared with WS04, WS07, and WS19. Instead, a faster response with higher event water contribution was noted in WS19 (constantly grazed short grass, compacted topsoil layer with low infiltration, storage and interception compared with natural grass).

Another factor that might explain the differences in pre-event water between the Maimai and H. J. Andrews catchment and the Zwäckentobel, are the different subsurface characteristics. The vertical cracks of the Maimai and more permeable soil types of the H. J. Andrews facilitate rain water infiltration and fill up the subsurface topography resulting in a subsurface threshold with dominant pre-event water. The Zwäckentobel instead has shallow gleysols with a low matrix permeability, small active storage, and dominant stormflow in the organic soil horizon (20–50 cm), similar to the soils of a nearby hillslope described by Schneider *et al.* (2014). In the Zwäckentobel, a typical riparian zone was lacking but the large areas of wetlands were prominent elements of passive storage (Fischer *et al.* 2015). These elements are activated during the rainfall events and release the stored pre-event water. With increasing rainfall sum, at approximately 50 mm, a change from pre-event dominated to event dominated runoff was found (Figure 10). Hydrometric and isotopic observations of the soil profile were missing. However, we hypothesize that with increasing rainfall the shallow soils saturate and reach, at approximately 50 mm, the maximum storage capacity of the soil (in agreement with soil water retention and moisture information before and during plot scale sprinkling experiments by Feyen *et al.* (1996, 1999)). As a result, the distributed wetlands fully connect through preferential flowpaths (creeping soils, animal burrows, or old roots and ephemeral streams), any additional rainfall by-passes the shallow soils and participates in streamflow. This would explain that with increasing precipitation, the amount of runoff produced by the precipitation increases and the fraction of pre-event water decreased. The variable rainfall with additional small storage (organic soil horizon, 20–50 cm) results in a near surface-dependent threshold with subsequently more variable pre-event water contribution, showing similarities to the Babinda model described by Bonell *et al.* (1998). The connectivity of distributed wetlands is better described by the hydrogeomorphic model of Sidle *et al.* (2000), where spatially distributed passive sources progressively become active and connected with the flow network.

Beside the previously described implicit role of catchment characteristics in runoff processes, no relationship between the fraction of pre-event water and catchment characteristics was found in WS04–WS19 or the study of Burch *et al.* (1996) or Taylor & Pearce (1982). A reason could be that in events where observations (stream response and runoff processes) and explanatory variables (precipitation and catchment characteristics) are both spatially variable, it is difficult to determine the dominant influencing factor on runoff processes. Furthermore, it was likely that the frequent precipitation together with the catchment characteristics meant that the headwater was in a continuous wet state; therefore, any potential influence of catchment characteristics on runoff processes was not visible in the data. A similar reduced effect of wet antecedent conditions and flow through the upper soil horizon was observed by Shanley *et al.* (2002). This may also explain why, despite each event having different antecedent wetness conditions, no clear

relation of pre-event water contribution and antecedent proxies was observed. This is opposite to the findings of Shanley *et al.* (2002), Casper *et al.* (2003), Pellerin *et al.* (2008) and James & Roulet (2009). Furthermore, we did not observe a seasonal change in fraction of pre-event water as had been observed in different pre-alpine headwaters (McGuire & McDonnell 2010; Penna *et al.* 2014).

The IHS gave good qualitative information on the contribution of rainfall and the fraction of pre-event water, nevertheless many questions on the flowpath, the runoff (Lyon *et al.* 2008), and thresholds (Graham *et al.* 2010) are unresolved. Future studies should validate the connectivity, interaction, and different runoff processes of the headwater internal catchment elements (such as wetlands or forest). A multiple tracer approach (using similar tracers used by Fischer *et al.* (2015), $\delta^{18}O$, Ca and DOC) would allow better understanding of the flowpaths and contributing sources during stormflow of headwaters, while a finer temporal sampling resolution would help investigate subtle changes in pre-event water in relation to differences in catchment characteristics.

CONCLUSION

In this study, 13 rainfall–runoff events of different magnitude and intensity were analyzed in five neighboring steep and rainfall dominated headwaters, to assess the pre-event water contribution. The combination of long-term and spatially short-term hydrometeorological measurements, together with event water sampling in different neighboring streams and multiple events, complemented each other and helped to overcome individual limitations.

The pre-event water contribution was found to be temporally variable and depended on rainfall amount and intensity. Small events had high pre-event water contribution. With increasing precipitation, the volume of runoff produced by precipitation increased and a change from pre-event to event water dominated runoff processes occurred. The variable rainfall amount and small active storage (organic soil horizon, 20–50 cm) resulted in a threshold in the upper soil horizon with subsequently more variable pre-event water contribution.

Despite the differences in catchment characteristics between the neighboring streams at headwater scale, no significant difference in minimum fraction of pre-event water contribution was observed. Furthermore, none of the antecedent wetness proxies had any explanatory value on the minimum fraction of pre-event water. This can be explained by the frequent precipitation and by the catchment characteristics keeping the soil in a wet state.

In contrast to the conventional approach (i.e., studying one headwater with few events), our results highlight the necessity to study different neighboring headwaters and a wide range of event magnitudes (many events and many samples), to better understand the dynamic character and controlling factors in runoff processes.

ACKNOWLEDGEMENTS

We thank all the people who helped in the field and the laboratory. Especially we thank Ilaria Clemenzi, Michael Rinderer, Martin Šanda, Russel Smith, Stefan Plötner, Stephan Müller, Karl Steiner, Andrea Kolleger, Ellen Cerwinka, Sandra Pool, Sandra Schärer, Nadja Lavanga, Seraina Kauer, Jana Dusik, Paribesh Pradhan, Andrea Ruecker, Yves Götz, Annagreth Schuler and Werni Ruhstaller, Bruno Kägi, Claudia Schreiner, Michael Hilf, Sandra Röthlisberger, and Ivan Woodhatch. We thank Tracy Ewen for proofreading the manuscript, the editor and two anonymous reviewers provided helpful comments, which helped to clarify the text. We also thank the Oberallmeindkorporation Schwyz (OAK), the Department of Environment of the Canton of Schwyz and the municipality Alpthal for their helpful cooperation.

REFERENCES

Allen, S. T., Keim, R. F. & McDonnell, J. J. 2015 Spatial patterns of throughfall isotopic composition at the event and seasonal timescales. *J. Hydrol.* **522**, 58–66.

Blume, T., Zehe, E. & Bronstert, A. 2007 Rainfall–runoff response, event-based runoff coefficients and hydrograph separation. *Hydrol. Sci. J.* **52**, 843–862.

Bonell, M., Pearce, A. J. & Stewart, M. K. 1990 The identification of runoff-production mechanisms using environmental isotopes in a tussock grassland catchment, eastern Otago, New Zealand. *Hydrol. Processes* **4**, 15–34.

Bonell, M., Barnes, C. J., Grant, C. R., Howard, A. & Burns, J. 1998 High rainfall, response-dominated catchments: A comparative study of experiments in tropical northeast Queensland with temperate New Zealand. In: *Isotope Tracers in Catchment Hydrology* (C. Kendall & J. J. McDonnell, eds) Elsevier, Amsterdam, The Netherlands, pp. 347–390.

Brown, V. A., McDonnell, J. J., Burns, D. A. & Kendall, C. 1999 The role of event water, a rapid shallow flow component, and catchment size in summer stormflow. *J. Hydrol.* **217** (3–4), 171–190.

Burch, H., Forster, F. & Schleppi, P. 1996 Zum Einfluss des Waldes auf die Hydrolgie der Flysch-Einzugsgebiete des Alptals. [The influence of the forest on the hydrology of flysch basins of the Alptals]. *Swiss J. For.* **12**, 925–938.

Burns, D. A. 2002 Stormflow-hydrograph separation based on isotopes: the thrill is gone – what's next? *Hydrol. Processes* **16**, 1515–1517.

Buttle, J. M. 1994 Isotope hydrograph separations and rapid delivery of pre-event water from drainage basins. *Prog. Phys. Geogr.* **18**, 16–41.

Casper, M. C., Volkmann, H. N., Waldenmeyer, G. & Plate, E. J. 2003 The separation of flow pathways in a sandstone catchment of the northern Black Forest using DOC and a nested approach. *Phys. Chem. Earth Parts A/B/C* **28**, 269–275.

Feyen, H., Leuenberger, J., Papritz, A., Gysi, M., Flühler, H. & Schleppi, P. 1996 Runoff processes in catchments with a small scale topography. *Phys. Chem. Earth* **21**, 177–181.

Feyen, H., Wunderli, H., Wydler, H. & Papritz, A. 1999 A tracer experiment to study flow paths of water in a forest soil. *J. Hydrol.* **225**, 155–167.

Fischer, B. M. C., Rinderer, M., Schneider, P., Ewen, T. & Seibert, J. 2015 Contributing sources to baseflow in pre-alpine headwaters using spatial snapshot sampling. *Hydrol. Processes* **29**, 5321–5336.

Genereux, D. 1998 Quantifying uncertainty in tracer-based hydrograph separations. *Water Resour. Res.* **34**, 915–919.

Geris, J., Tetzlaff, D., McDonnell, J. & Soulsby, C. 2015 The relative role of soil type and tree cover on water storage and transmission in northern headwater catchments. *Hydrol. Processes* **29** (7), 1844–1860.

Gerrits, A. M. J., Pfister, L. & Savenije, H. H. G. 2010 Spatial and temporal variability of canopy and forest floor interception in a beech forest. *Hydrol. Processes* **24** (21), 3011–3025.

Goodrich, D. C., Faurès, J.-M., Woolhiser, D. A., Lane, L. J. & Sorooshian, S. 1995 Measurement and analysis of small-scale convective storm rainfall variability. *J. Hydrol.* **173**, 283–308.

Graham, C. B., Woods, R. A. & McDonnell, J. J. 2010 Hillslope threshold response to rainfall: (1) a field based forensic approach. *J. Hydrol.* **393**, 65–76.

Gurtz, J., Baltensweiler, A. & Lang, H. 1999 Spatially distributed hydrotope-based modelling of evapotranspiration and runoff in mountainous basins. *Hydrol. Processes* **13**, 2751–2768.

Hagedorn, F., Bucher, J. B. & Schleppi, P. 2001 Contrasting dynamics of dissolved inorganic and organic nitrogen in soil and surface waters of forested catchments with Gleysols. *Geoderma* **100**, 173–192.

Hantke, R. 1967 Geological map of the Canton of Zurich and its neighboring areas. *Q. J. Nat. Hist. Soc. Zurich.*

Hegg, C., McArdell, B. W. & Badoux, A. 2006 One hundred years of mountain hydrology in Switzerland by the WSL. *Hydrol. Processes* **20**, 371–376.

Hinton, M. J., Schiff, S. L. & English, M. C. 1994 Examining the contributions of glacial till water to storm runoff using two- and three-component hydrograph separations. *Water Resour. Res.* **30** (4), 983–993.

Holko, L., Dóša, M., Michalko, J. & Kostka, Z. 2012 Isotopes of oxygen-18 and deuterium in precipitation in Slovakia. *J. Hydrol. Hydromech.* **60**, 265–276.

Hrachowitz, M., Bohte, R., Mul, M. L., Bogaard, T. A., Savenije, H. H. G. & Uhlenbrook, S. 2011 On the value of combined event runoff and tracer analysis to improve understanding of catchment functioning in a data-scarce semi-arid area. *Hydrol. Earth Syst. Sci.* **15**, 2007–2024.

Hsü, K. J. & Briegel, U. (eds) 1991 The flysch. In: *Geology of Switzerland*. Birkhäuser, Basel, Switzerland, pp. 65–82.

James, A. L. & Roulet, N. T. 2009 Antecedent moisture conditions and catchment morphology as controls on spatial patterns of runoff generation in small forest catchments. *J. Hydrol.* **377**, 351–366.

Jordan, J. P. 1994 Spatial and temporal variability of stormflow generation processes on a Swiss catchment. *J. Hydrol.* **153**, 357–382.

Keller, H. M. 1970 Factors affecting water quality of small mountain catchments. *J. Hydrol.* **9**, 133–141.

Kennedy, V. C., Zellweger, G. W. & Avanzino, R. J. 1979 Variation of rain chemistry during storms at two sites in northern California. *Water Resour. Res.* **15**, 687–702.

Kienzler, P. M. & Naef, F. 2008 Subsurface storm flow formation at different hillslopes and implications for the 'old water paradox'. *Hydrol. Processes* **116**, 104–116.

Klaus, J. & McDonnell, J. J. 2013 Hydrograph separation using stable isotopes: review and evaluation. *J. Hydrol.* **505**, 47–64.

Laudon, H., Sjöblom, V., Buffam, I., Seibert, J. & Mörth, M. 2007 The role of catchment scale and landscape characteristics for runoff generation of boreal streams. *J. Hydrol.* **344**, 198–209.

Lis, G., Wassenaar, L. I. & Hendry, M. J. 2008 High-precision laser spectroscopy D/H and 18O/16O measurements of microliter natural water samples. *Anal. Chem.* **80** (1), 287–293.

Lyon, S. W., Desilets, S. L. E. & Troch, P. A. 2008 Characterizing the response of a catchment to an extreme rainfall event using hydrometric and isotopic data. *Water Resour. Res.* **44**, W06413.

Lyon, S. W., Desilets, S. L. E. & Troch, P. A. 2009 A tale of two isotopes: differences in hydrograph separation for a runoff event when using δD versus δ18O. *Hydrol. Processes* **23** (14), 2095–2101.

McCartney, M. P., Neal, C. & Neal, M. 1998 Use of deuterium to understand runoff generation in a headwater catchment containing a dambo. *Hydrol. Earth Syst. Sci.* **2**, 65–76.

McDonnell, J. J., Bonell, M., Stewart, M. K. & Pearce, A. J. 1990 Deuterium variations in storm rainfall: implications for

stream hydrograph separation. *Water Resour. Res.* **26**, 455–458.

McGlynn, B. L., McDonnel, J. J. & Brammer, D. D. 2002 A review of the evolving perceptual model of hillslope flowpaths at the Maimai catchments, New Zealand. *J. Hydrol.* **257**, 1–26.

McGlynn, B. L., McDonnell, J. J., Seibert, J. & Kendall, C. 2004 Scale effects on headwater catchment runoff timing, flow sources, and groundwater-streamflow relations. *Water Resour. Res.* **40**, W07504.

McGuire, K. J. & McDonnell, J. J. 2010 Hydrological connectivity of hillslopes and streams: characteristic time scales and nonlinearities. *Water Resour. Res.* **46** (10), W10543.

Menzel, L., Lang, H. & Martin, R. 2007 Mean annual actual evaporation 1973–1992. *Hydrol. Atlas Switz*. Federal Office for the Environment FOEN, Bern.

Molnar, P., Densmore, A. L., McArdell, B. W., Turowski, J. M. & Burlando, P. 2010 Analysis of changes in the step-pool morphology and channel profile of a steep mountain stream following a large flood. *Geomorphology* **124**, 85–94.

Onda, Y., Tsujimura, M., Fujihara, J. & Ito, J. 2006 Runoff generation mechanisms in high-relief mountainous watersheds with different underlying geology. *J. Hydrol.* **331**, 659–673.

Pearce, A. J. 1990 Streamflow generation processes: an Austral view. *Water Resour. Res.* **26**, 3037–3047.

Pellerin, B. A., Wollheim, W. M., Feng, X. & Vörösmarty, C. J. 2008 The application of electrical conductivity as a tracer for hydrograph separation in urban catchments. *Hydrol. Processes* **22**, 1810–1818.

Penna, D., Stenni, B., Šanda, M., Wrede, S., Bogaard, T. A., Gobbi, A., Borga, M., Fischer, B. M. C., Bonazza, M. & Chárová, Z. 2010 On the reproducibility and repeatability of laser absorption spectroscopy measurements for δ2H and δ18O isotopic analysis. *Hydrol. Earth Syst. Sci.* **14**, 1551–1566.

Penna, D., van Meerveld, H. J., Oliviero, O., Zuecco, G., Assendelft, R. S., Dalla Fontana, G. & Borga, M. 2014 Seasonal changes in runoff generation in a small forested mountain catchment. *Hydrol. Processes* **29**, 2027–2042.

Renshaw, C. E., Feng, X., Sinclair, K. J. & Dums, R. H. 2003 The use of stream flow routing for direct channel precipitation with isotopically-based hydrograph separations: the role of new water in stormflow generation. *J. Hydrol.* **273**, 205–216.

Rinderer, M., Kollegger, A., Fischer, B. M. C., Stähli, M. & Seibert, J. 2012 Sensing with boots and trousers – qualitative field observations of shallow soil moisture patterns. *Hydrol. Processes* **26**, 4112–4120.

Roa-García, M. C. & Weiler, M. 2010 Integrated response and transit time distributions of watersheds by combining hydrograph separation and long-term transit time modeling. *Hydrol. Earth Syst. Sci.* **14**, 1537–1549.

Rodhe, A. 1987 *The Origin of Streamwater Traced by Oxygen-18*. University of Uppsala, Sweden.

Saxena, R. 1987 Oxygen-18 fractionation in nature and estimation of groundwater recharge. University of Uppsala.

Schneider, P., Pool, S., Strouhal, L. & Seibert, J. 2014 True colors – experimental identification of hydrological processes at a hillslope prone to slide. *Hydrol. Earth Syst. Sci.* **18** (2), 875–892.

Segura, C., James, A. L., Lazzati, D. & Roulet, N. T. 2012 Scaling relationships for event water contributions and transit times in small-forested catchments in Eastern Quebec. *Water Resour. Res.* **48** (7), W07502.

Shanley, J. B., Kendall, C., Smith, T. E., Wolock, D. M. & McDonnell, J. J. 2002 Controls on old and new water contributions to stream flow at some nested catchments in Vermont, USA. *Hydrol. Processes* **16** (3), 589–609.

Sidle, R. C., Tsuboyama, Y., Noguchi, S., Hosoda, I., Fujieda, M. & Shimizu, T. 2000 Stormflow generation in steep forested headwaters: a linked hydrogeomorphic paradigm. *Hydrol. Processes* **14** (3), 369–385.

Sklash, M. G. & Farvolden, R. N. 1979 The role of groundwater in storm runoff. *J. Hydrol.* **43**, 45–65.

Sklash, M. G., Farvolden, R. N. & Fritz, P. 1976 A conceptual model of watershed response to rainfall, developed through the use of oxygen-18 as a natural tracer. *Can. J. Earth Sci.* **13**, 271–283.

Stähli, M. & Gustafsson, D. 2006 Long-term investigations of the snow cover in a subalpine semi-forested catchment. *Hydrol. Processes* **20**, 411–428.

Suecker, J. K., Ryan, J. N., Kendall, C. & Jarrett, R. D. 2000 Determination of hydrologic pathways during snowmelt for alpine/subalpine basins, Rocky Mountain National Park, Colorado. *Water Resour. Res.* **36** (1), 63–75.

Taylor, C. H. & Pearce, A. J. 1982 Storm runoff processes and subcatchment characteristics in a New Zealand hill country catchment. *Earth Surf. Processes Landforms* **7**, 439–447.

Turowski, J. M., Yager, E. M., Badoux, A., Rickenmann, D. & Molnar, P. 2009 The impact of exceptional events on erosion, bedload transport and channel stability in a step-pool channel. *Earth Surf. Processes Landforms* **34**, 1661–1673.

Vitvar, T. & Balderer, W. 1997 Estimation of mean water residence times and runoff generation by180 measurements in a Pre-Alpine catchment (Rietholzbach, Eastern Switzerland). *Appl. Geochem.* **12**, 787–796.

Wassenaar, L. I., Coplen, T. B. & Aggarwal, P. K. 2014 Approaches for achieving long-term accuracy and precision of δ18O and δ2H for waters analyzed using laser absorption spectrometers. *Environ. Sci. Technol.* **48** (2), 1123–1131.

Weiler, M., Naef, F. & Leibundgut, C. 1998 Study of runoff generation on hillslopes using tracer experiments and a physically based numerical hillslope model. *IAHS* **248**, 353–362.

Weiler, M., Scherrer, S., Naef, F. & Burlando, P. 1999 Hydrograph separation of runoff components based on measuring hydraulic state variables, tracer experiments, and weighting methods. *IAHS* **258**, 249–255.

First received 8 September 2015; accepted in revised form 22 December 2015. Available online 12 February 2016